Seasonal COP of a residential magnetocaloric heat pump based on MnFePSi

Pineda Quijano, Diego; Fonseca Lima, Beatriz; Infante Ferreira, Carlos; Brück, Ekkes

DOI
10.1016/j.ijrefrig.2024.04.014

Publication date
2024

Document Version
Final published version

Published in
International Journal of Refrigeration

International Journal of Refrigeration 164 (2024) 38–48

Contents lists available at ScienceDirect

International Journal of Refrigeration

journal homepage: www.elsevier.com/locate/ijrefrig

Seasonal COP of a residential magnetocaloric heat pump based on MnFePSi
COP saisonnier d'une pompe à chaleur magnétocalorique à base de matériaux MnFePSi

Diego Pineda Quijano [a,b,*], Beatriz Fonseca Lima [c], Carlos Infante Ferreira [b], Ekkes Brück [a,**]

[a] Fundamental Aspects of Materials and Energy, Department of Radiation Science and Technology, TU Delft, Mekelweg 15, 2629 JB, Delft, The Netherlands
[b] Process and Energy Laboratory, Delft University of Technology, Leeghwaterstraat 39, 2628 CB, Delft, The Netherlands
[c] Faculty of Engineering, University of Porto, Rua Dr. Roberto Frias, s/n, 4200-465, Porto, Portugal

ARTICLE INFO

Keywords:
Magnetocaloric heat pump
Seasonal COP
Layered AMR
MnFePSi
Numerical simulation

Mots clés:
Pompe à chaleur magnétocalorique
COP saisonnier
AMR en couches
MnFePSi
Simulation numérique

ABSTRACT

The performance of a magnetocaloric heat pump (MCHP) consisting of active magnetocaloric regenerators (AMR) of 12 layers of MnFePSi magnetocaloric materials (MCM) with a linear distribution of Curie temperatures was investigated using a 1D numerical model. The model predicted the heating power and coefficient of performance (COP) of the AMR for a fixed temperature span of 27 K, between 281 K and 308 K, and variable flow rate and AMR cycle frequency. A maximum applied magnetic field strength of 1.4 T was used. A well-insulated house with a maximum heating power demand of 3 kW (under quasi steady state conditions) was considered. Ambient temperature in The Netherlands was taken as a reference for the estimation of the seasonal heating power demand. Without optimizing the design of the AMR, the model predicts a maximum single-AMR heating power equal to 43.5 W when the AMR operates at 3 Hz and 3 L min^{-1}, and a maximum COP equal to 5.8 when it operates at 1.5 Hz and 1 L min^{-1} Considering the maximum heating power of a single AMR, approximately 69 AMRs are needed to provide the design heating power demand of the house. It was found that it is possible to achieve an AMR seasonal COP of 5.6 by continuously adjusting the flow rate and frequency of operation of the MCHP along with the ON/OFF switching of some groups of AMRs in order to adjust the heating power of the MCHP to the heating power demand of the house.

1. Introduction

The International Energy Agency (IEA) estimated that by 2020 only about 10% of the worldwide heating needs of buildings were supplied by heat pumps. The IEA also estimated that this figure has to increase to at least 20% by 2030 in order to meet the climate goals (Cozzi et al., 2022). Aligned with these ambitions, the European Union (EU) has targeted to deploy 30 million units of heat pumps between 2022 and 2030 (Cozzi et al., 2022) and at the same time has enforced more stringent legislation regarding the use of refrigerants with high global warming potential (Environmental Investigation Agency, 2015). This is consistent with the ambitious emission reduction plans, but it also represents a challenge for manufacturers and end users. The EU is also stimulating the development of new heat pumping technologies (see for example EU, 2023). Among the technologies that are currently under development, the magnetocaloric heat pumping technology was classified by the US Department of Energy as one of the non-vapour compression "very promising" technologies with high energy savings potential that offers a non-energy related benefit such as noise reduction. However, it is still poorly rated regarding cost and complexity (Goetzler et al., 2014).

1.1. Magnetocaloric heat pumps

Magnetocaloric heat pumps (MCHP) generally consist of three main elements: a porous structure of magnetocaloric material (MCM), a type of compound that exhibits a thermal response when subjected to a magnetic field change known as the magnetocaloric effect (MCE); a magnetic field source such as a permanent magnet to trigger the MCE; and a heat transfer fluid (HTF) that flows through the porous structure of MCM and through external heat exchangers transporting heat from the cold to the hot side of the heat pump in this process. The porous structure of MCM is known as active magnetocaloric regenerator (AMR) and has the double function of regenerator and solid refrigerant. The HTF flows in a reciprocating manner in the AMR, and as a result a

* Corresponding author at: Process and Energy Laboratory, Delft University of Technology, Leeghwaterstraat 39, 2628 CB, Delft, The Netherlands.
** Corresponding author.
E-mail addresses: D.F.PinedaQuijano@tudelft.nl (D. Pineda Quijano), C.A.InfanteFerreira@tudelft.nl (C. Infante Ferreira), E.H.Bruck@tudelft.nl (E. Brück).

https://doi.org/10.1016/j.ijrefrig.2024.04.014
Received 23 November 2023; Received in revised form 5 April 2024; Accepted 21 April 2024
Available online 24 April 2024

Nomenclature

Variables

A	Area (m^2)
c	Specific heat capacity ($J\,kg^{-1}\,K^{-1}$)
COP	Coefficient of performance (-)
f	Frequency (Hz)
H	Magnetic field ($A\,m^{-1}$)
h	Heat transfer coefficient ($W\,m^{-2}\,K^{-1}$)
k	Thermal conductivity ($W\,m^{-1}\,K^{-1}$)
L	Length (m)
$\dot{m}$	Mass flow rate ($kg\,s^{-1}$)
P	Pressure (Pa)
$\dot{Q}$	Heat transfer rate (W)
s	Specific entropy ($J\,kg^{-1}\,K^{-1}$)
T	Temperature (K)
t	Time (s)
U	Overall heat transfer coefficient ($W\,m^{-2}\,K^{-1}$)
x	Axial position (m)

Greek symbols

β	Specific surface area ($m^2\,m^{-3}$)
Δ	Difference (-)
ρ	Density ($kg\,m^{-3}$)
τ	Cycle period (s)
ε	Porosity (-)
φ	Utilization (-)

Subscripts

ad	Adiabatic
amb	Ambient
AMR	Active magnetocaloric regenerator
c	Cold
cs	Cross section
eff	Effective
f	Fluid
h	Hot
mag	Magnetic
out	Outdoor
room	Room
s	Solid
span	span

Abbreviations

AMR	Active magnetocaloric regenerator
COP	Coefficient of performance
GSHEX	Ground source heat exchanger
HTF	Heat transfer fluid
KNMI	Koninklijk Nederlands Meteorologisch Instituut
MCE	Magnetocaloric effect
MCHP	Magnetocaloric heat pump
MCM	Magnetocaloric material
PID	Proportional-Integral-Derivative controller
RVO	Rijksdienst voor Ondernemend Nederland
SCOP	Seasonal coefficient of performance
UFH	Underfloor heating

temperature gradient is established between the two ends of the AMR, from approximately the temperature of the cold reservoir to approximately the temperature of the hot reservoir. Consequently, the MCM in every section of the AMR undergoes a unique thermodynamic cycle in a different temperature range. As the MCE (expressed as an adiabatic temperature change or an isothermal entropy change when the material undergoes a magnetic field change) peaks near the Curie temperature of the MCM and given that this peak occurs in a narrow temperature range in (first order) materials such as LaFeSi and MnFePSi, the most promising material families for commercial MCHP systems, the use of several of these materials in a layered bed configuration is necessary to expand the temperature range of operation of the AMR and to align as much as possible the Curie temperature of every material with the actual temperatures around which it cycles (Pineda Quijano et al., 2023).

The magnetocaloric refrigeration cycle consists of four steps: magnetization, iso-field cooling (also known as cold-to-hot blow of HTF), demagnetization, and iso-field heating (also known as hot-to-cold blow of HTF). Depending on the synchronization between the magnetic field change and the flow of HTF, the magnetization and demagnetization processes can be adiabatic, isothermal, or somewhere in between, producing a Brayton-like cycle, an Ericsson-like cycle, or a cycle in between Brayton and Ericsson respectively (Kitanovski et al., 2015; Plaznik et al., 2013; Romero Gómez et al., 2013). The working principle of MCHPs and AMRs has been extensively reported, and the interested reader is referred to the work of Kitanovski et al. (2015), Smith et al. (2012), and Trevizoli et al. (2016a) for further and detailed explanation.

The magnetocaloric device described above can be used for cooling and heating applications. Magnetocaloric heat pumps and refrigerators operate under the same working principle and could be regarded as the same device just as vapour compression heat pumps and refrigerators. The use of one or the other term depends mainly on the purpose of use of the device. In general, in both technologies, refrigerators and heat pumps use different refrigerants because the selection of the refrigerant(s) depends on the working temperature range of the device.

1.2. MCHPs for the built environment

This article focuses on the application of the magnetocaloric technology for heating in the built environment. Johra et al. (2018) proposed an MCHP system consisting of a ground-source heat exchanger (GSHEX) used as heat source, connected in a single hydraulic circuit, i.e. without intermediate heat exchangers and using a single recirculation pump, to the MCHP and to an underfloor heating (UFH) system used as heat sink. Using a GSHEX is advantageous for any type of heat pump given that the temperature of the ground is higher than ambient temperature in the coldest months of the heating season and fluctuates less throughout the year. On the other hand, an UFH system can operate at lower temperatures in comparison with radiators while providing comfort to the occupants of the house, which is also beneficial for any type of heat pump given that smaller temperature spans are linked to higher efficiencies.

Another possible system configuration includes intermediate heat exchangers between the MCHP and the external heat exchangers, which has advantages and disadvantages. On the positive side, it may provide increased flexibility in the design of the GSHEX and UFH systems and higher controllability at part-load conditions in comparison with the single hydraulic loop case. For the system configuration without intermediate heat exchangers, the UFH system and the GSHEX must be designed to manage larger flow rates and smaller fluid temperature drops compared to a normal design given that the temperature

difference between outgoing and returning flows of an MCHP is usually of the order of magnitude of the adiabatic temperature change of the MCM (between 2 to 3 K). Separating the MCHP from the external heat exchangers also minimizes the risk of contamination of the HTF that flows through the AMRs. Furthermore, the HTF that flows through the MCHP needs some special additives to avoid corrosion of the MCM and freezing, so minimizing its volume is convenient. One disadvantage of the system configuration with intermediate heat exchangers is that the entropy production increases, and thus the overall efficiency of the heat pump reduces.

1.3. Capacity control of MCHPs

Part load control of heat pump systems is an issue of great importance. The main reason is that the heat pump has to be designed for peak load, but it operates most of the time at part-load conditions. MCHPs in particular have the advantage that the COP is larger at part-load conditions even when they operate at a fixed temperature span (Masche et al., 2023; Pineda Quijano et al., 2023; Qian et al., 2018). Therefore, a good control strategy is necessary to exploit this advantage in order to maximize their seasonal coefficient of performance (SCOP).

A few capacity control strategies have been proposed for MCHP systems, ranging from simple ON/OFF to feedback controllers. Johra et al. (2018) proposed to control the capacity of an MCHP by operating at a constant cycle frequency of 1 Hz and a variable flow rate. They simulated a house of nine rooms, every one of which was equipped with an independent UFH circuit that was switched ON and OFF to maintain a desired temperature in the room. The total flow rate of the MCHP changed in discrete steps depending on the number of UFH circuits demanding warm water. When none of the UFH circuits was demanding warm water, the MCHP and the circulation pump were turned OFF. When considering a room temperature of 22 °C, an undisturbed ground temperature of 10 °C, and the Danish weather conditions for the months January to April 2013, they calculated an AMR SCOP of 3.93 and a corresponding system SCOP of 1.84. The difference between these two results originated from running a centrifugal pump far from its optimum operating region.

To reduce the difference between AMR and system SCOP, the same research group proposed later an ON/OFF control strategy whereby the MCHP was operated most of the time at the flow rate that produced the maximum COP (for the same cycle frequency of 1 Hz) and the thermal mass of the house was used to store the excess energy supplied by the heat pump. The average temperature inside the house (calculated as the weighted average using the floor area of the rooms as weighting parameter) was allowed to fluctuate between an upper and a lower limit. When these limits were reached, the MCHP was switched OFF and ON respectively. When a particular room reached the upper temperature limit the corresponding UFH circuit was closed and the total flow rate of the MCHP decreased, moving the heat pump from its optimum performance point. When considering an upper/lower limit temperature difference of 4 K and a house thermal inertia of 60 $\mathrm{W\,h\,K^{-1}\,m^{-2}}$, they found that the system operated at least 70% of the time at the optimum flow rate and the system SCOP increased to 3.48 (Johra et al., 2019). The disadvantage of this strategy is that the temperature fluctuation could bring discomfort to occupants.

Qian et al. (2018) proposed a feedback control system that used the AMR cycle frequency and utilization as control variables. Utilization is the ratio between the thermal mass of the fluid in a single blow and the thermal mass of the solid AMR. A PID controller determined the cycle frequency based on the assumption of a linear dependence of cooling power with AMR cycle frequency. Then, the HTF flow rate was calculated assuming a constant utilization value of 0.8 and using the frequency obtained from the PID controller. These two assumptions may not hold for all MCHP systems, but the overall control strategy offers great flexibility and allows the system to operate at a small fraction of the nominal cooling capacity with higher efficiency. Later, Qian et al. (2019) eliminated the second assumption, and, using numerical steady state simulations, they calculated the utilization value that maximizes COP for every frequency and temperature span considered in their parameter domain. Then, they used these optimum pre-calculated steady state operating points (frequency, utilization, temperature span) in the feedback loop to determine the optimum utilization value corresponding to every frequency obtained from the PID controller. An issue that we see in their approach and that was in fact causing problems in their control loop is that utilization is not a truly independent variable since it depends on flow rate as well as on frequency. So, using flow rate and frequency should be a better choice of control variables for this system.

Liang et al. (2022) suggested to control the capacity of an MCHP (designed to be used as a booster heat pump in an ultra-low-temperature district heating system) by continuously modulating the cycle frequency and the mass flow rate. Using steady state numerical simulations, they mapped the performance of the MCHP in terms of COP and heating power for a fixed temperature span. The authors found that simultaneously tuning frequency and flow rate enabled to reduce the heating power by 52.6% while increasing the COP by 68% compared to the full load condition. They also studied the effect of using the blow fraction and the offset fraction between magnetic and fluid flow profiles as capacity control variables, but they concluded that using cycle frequency and flow rate was more effective in terms of capacity reduction and efficiency increase.

Finally, Masche et al. (2023) proved experimentally that it is possible to tune the capacity of an MCHP by simultaneous modulation of the cycle frequency and HTF flow rate for a constant temperature span.

1.4. Goal and assumptions of this study

The previous literature study demonstrated the technical feasibility of the application of a MCHP for the built environment. However, none of the previous studies considered MnFePSi as the base material for the MCHP. Furthermore, a research study combining the lessons mentioned above has not yet been presented to the community. Therefore, the main goal of this study is to estimate the SCOP of an MCHP based on MnFePSi that provides heat to a house using a similar system configuration as the one proposed by Johra et al. (2018) and the part-load control strategy suggested by Qian et al. (2019) and Liang et al. (2022). This study is based on the following assumptions:

- It is assumed that the MCHP operates at a fixed temperature span, which is important for the activation of all layers in a layered AMR. This is approximately feasible for the adopted system configuration since the ground temperature is unaffected by ambient temperature fluctuations at depths below 10 m. However, ground temperature decreases over the heating season due to depletion of the geothermal reservoir (Shirazi and Bernier, 2013).
- AMR SCOP will be primarily reported rather than system SCOP given that only the AMR is modelled and therefore only intrinsic AMR power consumption is calculated. However, a system SCOP can be estimated by considering representative motor and drive train efficiencies as it will be shown.
- Since the attention is on the AMR performance, it is assumed that the external heat exchangers work as efficiently at part-load conditions as in full load operation. Further research is conducted at the moment to size these heat exchangers for a proper operation under off-design conditions.
- A well insulated house is assumed for the estimation of the heating power demand.
- Ambient temperature in the Netherlands in the heating season 2009/2010 (KNMI, 2010) is used as a reference for the estimation of the heating power demand.

2. Methods

For the estimation of the SCOP of an MCHP, we first mapped the performance of an AMR in terms of COP and heating power as a function of HTF flow rate and AMR cycle frequency for a fixed temperature span using a 1D numerical model. We used a modified version of the model implemented by Christiaanse (2019), which is documented in Refs. Christiaanse (2018) and Christiaanse et al. (2019). This model, as all one dimensional models, departs from the following general assumptions (Nielsen et al., 2011):

- In any cross sectional area of the AMR, the fluid velocity, the distribution of MCM, the magnetic field, and the fluid and solid temperatures are uniform.
- Only heat transfer by convection occurs between solid and fluid.
- The HTF remains in the liquid phase.

2.1. Governing equations

Eqs. (1) and (2) are the governing equations of the model and correspond to the energy balances of the fluid and solid domains of the AMR respectively. The fluid energy conservation equation considers the following physical phenomena from left to right: thermal energy storage, enthalpy transfer, axial diffusion, viscous dissipation, heat leaks from/to the environment, and heat transfer with the solid. On the other hand, as pointed out by Lei (2016), in the absence of irreversibilities the first two terms (inside parenthesis) on the left hand side of the solid energy conservation equation, Eq. (2), are equivalent to energy storage and magnetic work. The second term on the left hand side of Eq. (2) corresponds to diffusion in the solid phase, and the term on the right hand side is again the heat exchange between fluid and solid that couples the two equations.

$$\rho_f c_f A_{cs} \varepsilon \frac{\partial T_f}{\partial t} + \dot{m} \frac{\partial}{\partial x}\left(c_f T_f\right) - \frac{\partial}{\partial x}\left(k_{f,\mathrm{eff}} A_{cs} \varepsilon \frac{\partial T_f}{\partial x}\right) = \left|\frac{\dot{m}}{\rho_f}\frac{\partial P}{\partial x}\right| + \dot{Q}_{\mathrm{amb}} + A_{cs}\beta h(T_s - T_f) \tag{1}$$

$$\rho_s A_{cs}(1-\varepsilon)\left(c_s \frac{\partial T_s}{\partial t} + T_s\left(\frac{\partial s}{\partial H}\right)_{T_s}\frac{\partial H}{\partial t}\right) - \frac{\partial}{\partial x}\left(k_{s,\mathrm{eff}} A_{cs}(1-\varepsilon)\frac{\partial T_s}{\partial x}\right) = A_{cs}\beta h(T_f - T_s) \tag{2}$$

2.2. Constitutive equations

Constitutive equations were chosen assuming that the AMR consists of a packed bed of spherical particles. The Ergun equation was used for the calculation of viscous losses (Ergun, 1952). The heat transfer coefficient for the heat exchange between fluid and solid was calculated using a correlation derived by Macias-Machin et al. (1991). This heat transfer coefficient was multiplied by a degradation factor to account for temperature gradients inside the spherical particles, as proposed by Engelbrecht et al. (2006). The diffusion in the liquid phase (hydrodynamic dispersion) was calculated using an effective thermal conductivity, $k_{f,\mathrm{eff}}$ (Koch and Brady, 1985). The diffusion in the solid phase was calculated considering an effective thermal conductivity, $k_{s,\mathrm{eff}}$, using an equation proposed by Hadley (1986) to account for the presence of the fluid in the spaces between the solid particles.

2.3. Magnetocaloric materials

The MnFePSi family of MCMs was considered for this study. As the MCE peaks in a somewhat narrow temperature range in these materials (because they are first order MCMs), it is necessary to implement a layered AMR configuration, whereby materials with slightly different compositions and Curie temperatures are stacked one after another in the flow direction. Ideally, there should be a continuous change in Curie temperature along the AMR covering the temperature range of the MCHP to maximize the MCE at every axial position, which is analogous to use an infinite number of layers. However, this is still difficult to achieve in practice, and numerical simulations have also indicated that only a small number of layers is enough to achieve a performance comparable to that of a quasi-continuous layered AMR (Lei et al., 2016).

In an unpublished study, we also performed numerical simulations to determine the number of layers necessary to maximize the heating power of a layered AMR based on MnFePSi. We departed from the properties of the $Mn_{1.18}Fe_{0.73}P_{0.48}Si_{0.52}$ compound (see Ref. Christiaanse (2019)), the Curie temperature of which, given by the peak of the zero-field heat capacity, is approximately 293 K. Some relevant properties of this material are presented in Fig. 1. Then, we obtained the properties of the other materials in the simulated layered AMRs by shifting the properties of this base material to different Curie temperatures, i.e. the size and shape of the peaks (heat capacity, ΔT_{ad}, and Δs_{mag}) of each material in the simulated AMRs is the same but the temperature at which these peaks occur is different. We also considered an uniform layer length and a linear distribution of Curie temperatures for these AMRs. We concluded that under these considerations the heating power only increases marginally when the number of layers grows beyond 12. Therefore, we use an AMR of 12 layers in the present study. The peaks of the in-field heat capacity of these 12 MCMs span from 281 K to 308 K, the cold and hot reservoir temperatures of the heat pump respectively.

Table 1
Geometric parameters used in the simulated AMR.

Parameter	Value	Units
AMR W × H × L	45 × 13 × 60	mm × mm × mm
Porosity (ε)	0.36	–
Particle diameter	300	μm

2.4. Selected geometry

Table 1 summarizes the main geometric parameters concerning the AMR used in the simulations. The overall dimensions of this AMR coincide with the dimensions of the AMRs installed in the FAME cooler developed at TU Delft (Huang et al., 2019).

2.5. Magnetic field and fluid flow profiles

Fig. 2 shows the magnetic field and fluid flow profiles used in the simulations of this study. The magnetic field and fluid flow profiles are specific for every type of MCHP device and depend on the type of magnet and hydraulic circuit considered in the design of the MCHP. The shape of these profiles and their mutual synchronization determine the type of thermodynamic cycle that the MCMs undergo in the device (Plaznik et al., 2013). For the profiles presented in Fig. 2, the attainable thermodynamic cycles are close to Brayton-like cycles. These profiles are typical of devices using C-shaped, rotating magnets and rotating pumps such as the ones described in Refs. Aprea et al. (2014), Dall'Olio et al. (2021) and Huang et al. (2019). A maximum applied magnetic field strength of 1.4 T was selected to guarantee an adiabatic temperature change of more than 2 K for the selected MCM. This is also approximately the magnetic field strength of several pre-commercial prototypes (see for example Refs. Jacobs et al. (2013) and Dall'Olio et al. (2021)) and is closely related to the remanence of NdFeB, grade N50 magnets.

It is important to mention here that the blow fraction, defined as the ratio between the time the valves are open to flow in one direction and the cycle period, is the same for all simulations presented in this study. The blow fraction depends on the flow profile, but it is independent on

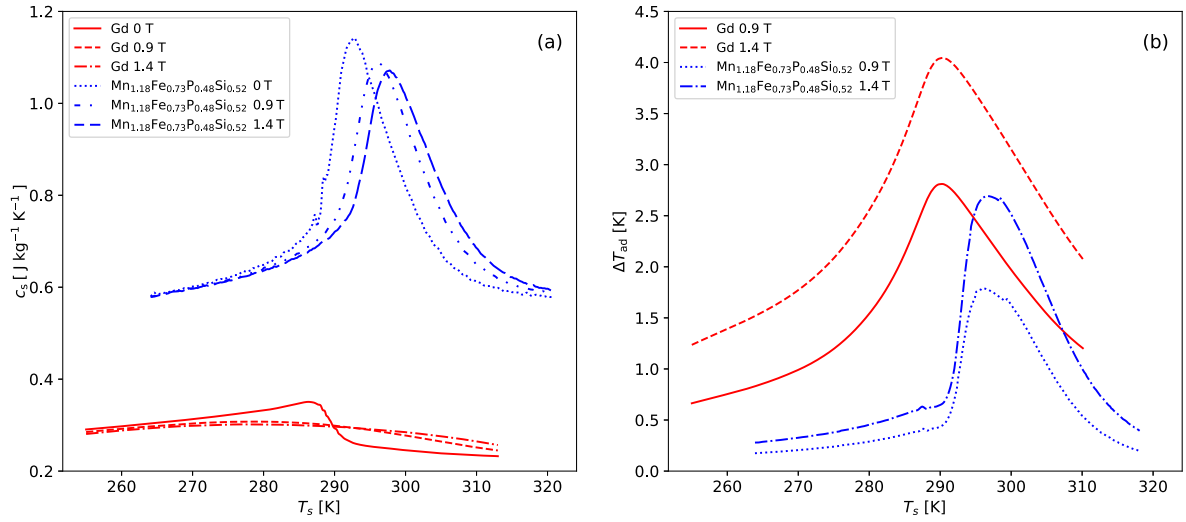

Fig. 1. Specific heat capacity (a) and adiabatic temperature change (b) of $Mn_{1.18}Fe_{0.73}P_{0.48}Si_{0.52}$ compared to those of Gd. Only heating curves are shown for the MnFePSi material.

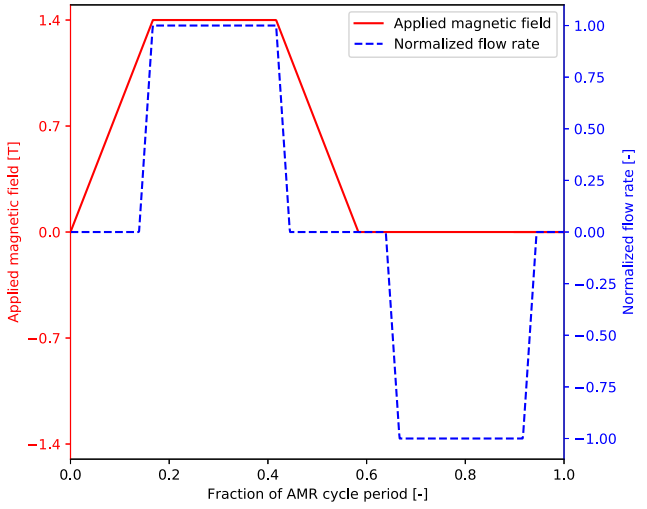

Fig. 2. Magnetic field and fluid flow profiles. These profiles resemble those of a C-shaped, rotating-magnet MCHP such as the one described in Huang et al. (2019).

the cycle frequency and maximum flow rate. The actual blow time does depend on cycle frequency. On the other hand, the volume displaced per blow process depends on the cycle frequency, maximum flow rate, and flow profile, and it corresponds to the area under the flow rate vs time profile. Some recent publications have considered the influence of flow profile on AMR performance as research topic (Fortkamp et al., 2018; Li et al., 2021; Vieira et al., 2023).

2.6. Performance metrics

The performance of the MCHP was evaluated in terms of the AMR heating power, calculated using Eq. (3), and AMR COP, calculated using Eq. (4). The AMR cooling power was calculated using Eq. (5).

$$\dot{Q}_h = \frac{1}{\tau}\int_0^{\tau} \dot{m} c_f (T_{f,x=L} - T_h)\, dt \tag{3}$$

$$COP = \frac{\dot{Q}_h}{\dot{Q}_h + \dot{Q}_{amb} - \dot{Q}_c} \tag{4}$$

$$\dot{Q}_c = \frac{1}{\tau}\int_0^{\tau} \dot{m} c_f (T_c - T_{f,x=0})\, dt \tag{5}$$

2.7. Solution, implementation, and validation

The governing equations were integrated using the finite difference method. The enthalpy term (also called advection by some authors) was discretized following an implicit upwind scheme. The diffusion terms were discretized using central difference in space and Crank–Nicolson in time. The solution of the system of algebraic equations for every time step is performed using the tridiagonal matrix algorithm. The model was implemented in Python. We validated the model with experimental data of a single AMR magnetocaloric refrigeration device that uses Gd as MCM (see Ref. Trevizoli et al. (2016b)) and obtained good agreement between experimental and numerical results (see Appendix). The original developers also validated the model with experiments of AMRs using two layers of MnFePSi (Christiaanse et al., 2018).

3. Results and discussion

3.1. Heating power demand

The calculation of the SCOP of a heat pump requires the definition of the part load heating demand. To do this, we follow a procedure similar to the one used in the European standard EN-14825:2022, "Air conditioners, liquid chilling packages and heat pumps, with electrically driven compressors, for space heating and cooling, commercial and process cooling - Testing and rating at part load conditions and calculation of seasonal performance". We adopted the average design (outdoor) and indoor temperatures of the EN-14825:2022, −10 °C and 20 °C respectively (European Committee for Standardization, 2022). At the design point, we assume that the heat pump unit has to deliver a heating power of 3 kW. The heating requirement of a Dutch terrace house built between 2015 and 2018 with improved insulation in windows and doors and improved infiltration sealing is 46.8 kW h m^{-2} per year (RVO, 2022). These houses are typically 117 m^2 (RVO, 2022). The heating system operates under average conditions 2066 h according to the EN-14825:2022. This gives an average heating power requirement of 2.65 kW, which indicates that our assumption is conservative. On the other hand, the EN-14825:2022 also considers a linear relationship between part-load heating demand and outdoor temperature. Following this, we consider a linear relationship between heating power demand and outdoor temperature by using Eq. (6).

$$\dot{Q}_h(t) = U A (T_{room} - T_{out}(t)) \tag{6}$$

The value of UA is assumed constant and is calculated at the design point where the heating power demand is 3 kW and the outdoor–indoor

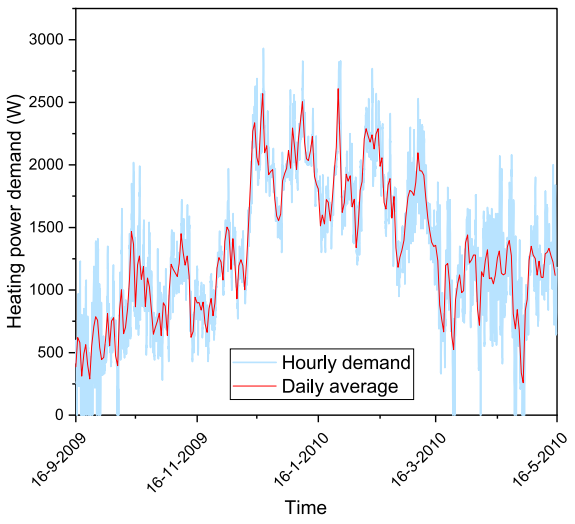

(a) Heating power demand profile

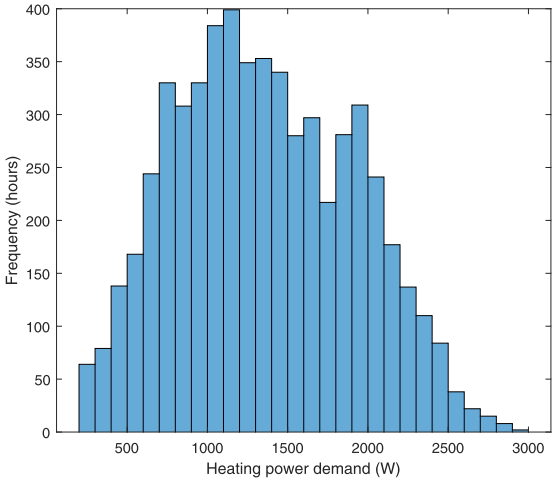

(b) Heating power demand distribution

Fig. 3. Heating power demand of a well insulated house characterized by $UA = 100\,\mathrm{W\,K^{-1}}$. Ambient temperature of the Netherlands in the heating season 2009/2010 is taken as a reference. Room temperature, T_{room}, is set to 20 °C.

temperature difference is 30 K, so UA is equal to $100\,\mathrm{W\,K^{-1}}$. The UA value of the Dutch house taken as a reference above is $68.62\,\mathrm{W\,K^{-1}}$, which results from the sum of the products of the U value (overall heat transfer coefficient) of the different building-envelope elements (such as external walls, roof, ground floor, windows, doors) times their corresponding areas (RVO, 2022). The value that we obtained, $100\,\mathrm{W\,K^{-1}}$, is therefore conservative as well. The difference can account for the extra load due to the ventilation/infiltration minus the internal heat gains. Ambient temperature in the Netherlands during the heating season of the years 2009/2010 was used as $T_{\mathrm{out}}(t)$ (KNMI, 2010). The heating season in the Netherlands is assumed here between the 16th of September to the 15th of May.

Fig. 3(a) shows the hourly and daily average heating power demand calculated using this approach. Fig. 3(b) shows, on the other hand, the distribution of heating power demand values. From Fig. 3(b), it is clear that the frequency of occurrence of the design heating power demand is very low and that the heating device has to operate most of the time at part-load conditions. For the calculation of the SCOP presented in Section 3.5, we excluded the hours in which $T_{\mathrm{out}} > 18\,°\mathrm{C}$ (104 h for the heating season of the years 2009/2010), for which the heating power demand is below 200 W according to Eq. (6). During the heating season under consideration, T_{out} was always larger than −10 °C, so the calculated heating power demand values are always below 3 kW.

3.2. AMR performance maps

Figs. 4(a) and 4(b) show respectively the heating power and COP developed by a 12-layer MnFePSi AMR as a function of AMR cycle frequency and fluid flow rate. A fixed temperature span of 27 K with $T_{\mathrm{c}} = 281\,\mathrm{K}$ and $T_{\mathrm{h}} = 308\,\mathrm{K}$ was considered here. As shown in Fig. 4(a), the maximum heating power that a single AMR can develop in the explored parameter space occurs in the upper limits of the range, $3\,\mathrm{L\,min^{-1}}$ and 3 Hz, and is about 43.5 W. Assuming that this is the design operating point, as many as 69 AMRs would be needed to supply the design heating power demand of 3 kW. Furthermore, taking into account that the mass of one AMR is approximately 137 g (considering a material density of $6100\,\mathrm{kg\,m^{-3}}$), the specific heating power of this AMR in the design point is approximately $318\,\mathrm{W\,kg^{-1}}$, which is in good agreement with the findings of Lei et al. (2016). The total mass of MCM needed is approximately 9.4 kg. On the other hand, the maximum COP of this AMR in the explored parameter space is approximately 5.8 and peaks at $1\,\mathrm{L\,min^{-1}}$, 1.5 Hz, where the heating power is only about 21 W. This trend is in agreement with the findings of other authors (see for example Ref. Liang et al. (2022)). As suggested by Qian et al. (2018), the fact that the AMR works more efficiently at part-load conditions can be exploited to increase the SCOP of an MCHP.

3.3. Part load control strategy

The performance maps shown in Figs. 4(a) and 4(b) are the base for the calculation of the SCOP for any part-load control strategy to be considered (Qian et al., 2019). As Liang et al. (2022) pointed out, the capacity of the AMR could be controlled by modulating only the flow rate and keeping frequency at maximum. Likewise, the heating power could also be controlled by fixing the flow rate at maximum and modulating frequency. However, none of these two paths leads to an optimum performance. Instead, a path that follows the operating points of maximum COP for every heating power could be chosen (Qian et al., 2019; Liang et al., 2022).

The blue line in Fig. 4(b) joints the points of maximum COP for every flow rate considered in the simulated parameter space. Fig. 5 also shows the values of the maximum COP calculated for every flow rate considered in the parameter space along with the corresponding frequency and heating power. Following this path of frequencies, the heating power of a single AMR increases monotonically with flow rate from approximately 11.7 W at $0.5\,\mathrm{L\,min^{-1}}$ to approximately 43.5 W at $3\,\mathrm{L\,min^{-1}}$. COP first increases from 5.2 to 5.8 for flow rates between $0.5\,\mathrm{L\,min^{-1}}$ and $1.0\,\mathrm{L\,min^{-1}}$ and then decreases monotonically with flow rate to reach a minimum value of 3.6 at $3\,\mathrm{L\,min^{-1}}$.

As mentioned above, for the selected geometry at least as many as 69 AMRs are necessary to satisfy the design heating power demand of 3 kW. If all 69 AMRs operate simultaneously, it is only possible to reduce the heating power down to 805 W by reducing the flow rate and AMR cycle frequency to the minimum values presented in Fig. 5. Flow rate and cycle frequency could be further reduced in theory to reach the minimum heating power demand of 200 W considered in this study, but in practice this is discouraged because reducing the speed of an electrical motor is in general inefficient.

Using a large number of AMRs offers an additional degree of freedom for the control of the capacity of the MCHP since the AMRs can be arranged in groups or modules each with an independent magnet and valve system that could be switched OFF as the heating power demand decreases. In this way the heating power of the MCHP could be further reduced below 805 W and down to 200 W.

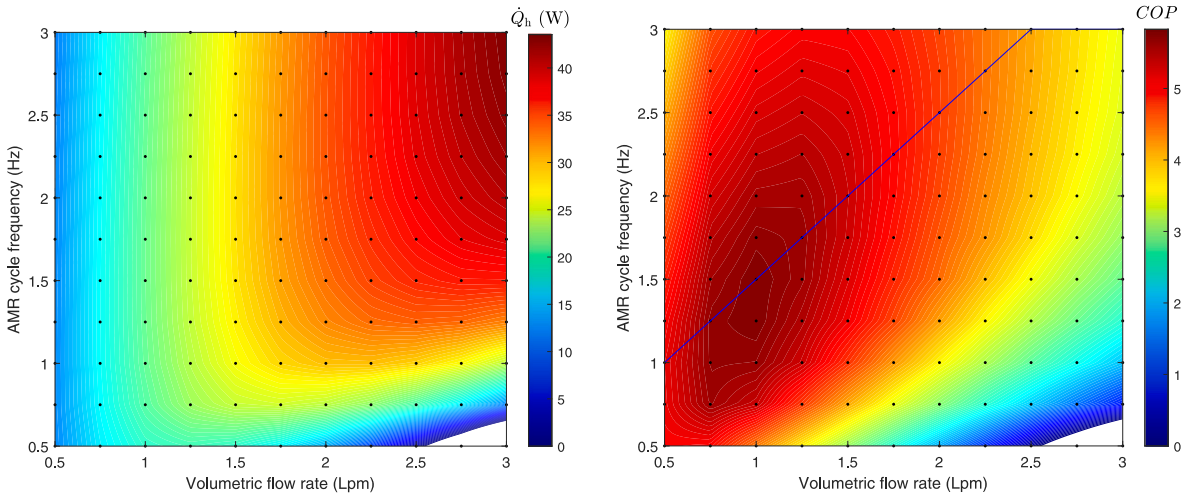

(a) Heating power [W] **(b)** Coefficient of Performance

Fig. 4. Heating power (a) and coefficient of performance (b) as a function of volumetric flow rate [Lpm] and AMR cycle frequency [Hz] of a single 12-layer MnFePSi AMR. $\Delta T_{span} = 27$ K. Black dots correspond to the simulated points. The blue line joints the points where COP is maximum for every flow rate.

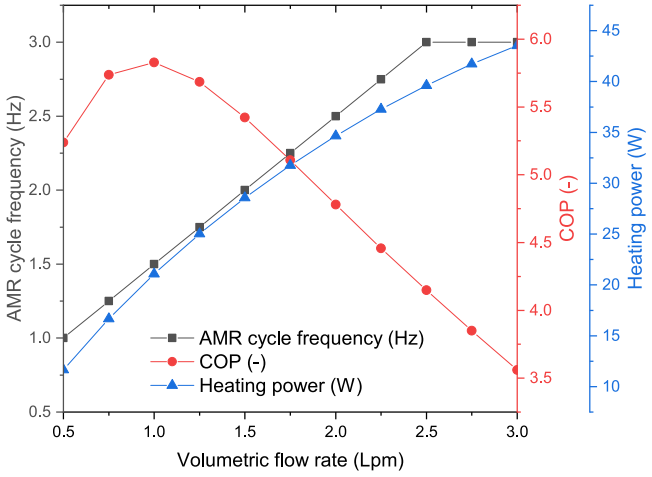

Fig. 5. Maximum COP calculated for every simulated flow rate and the corresponding frequency and heating power.

3.4. Modularization strategy

A large number of AMRs (such as 69) could be impractical to implement in a single-magnet configuration, and thus one of the options to obtain a simpler system could be to increase the mass of each AMR to reduce the total number. However, the optimization of the design of the AMRs was out of the scope of this article. The optimization of the dimensions of the AMR must be carried out in connection with the optimization of the design of the magnet assembly because the shape of the AMR is constrained by the dimensions of the air gap of the magnet. An example of such optimization process is presented in Lionte et al. (2021). These researchers used an evolutionary algorithm for the simultaneous optimization of the design of the magnet and AMRs. In our case, we decided to use the dimensions of the AMRs installed in the FAME cooler (Huang et al., 2019).

Another option for the implementation of a MCHP that uses several kilogrammes of MCM is to split the system in independent modules each with its own magnet and valve system. We selected this approach. We propose to split the system in 2 modules of 27 AMRs each plus one module of 15 AMRs. A subsystem of 27 AMRs is easier to achieve from a practical perspective compared to a single-magnet system that drives 69 AMRs.

Several examples of multi-bed AMR devices can be found in literature, some of which are summarized in Table 2. Single modules could follow the design of any of these prototypes, but the configurations that use magnetic assemblies with either concentric Halbach cylinders or magnetic rotor and iron stator with the AMRs placed in an annular space between inner and outer elements of the magnet assembly are more suitable to accommodate a large number of AMRs. The prototype developed by Engelbrecht et al. (2012) specially demonstrates that the implementation of a multi-bed system with 27 AMRs is technically feasible. Furthermore, it has also been shown that using an odd and large number of AMRs leads to a minimum torque (Wiesheu et al., 2023), which justifies the use of 27 AMRs. It is also important to highlight that the mass of the AMRs that we are considering in this article, 137 g, is of the same order of magnitude of the AMRs installed in the prototypes presented in Table 2. Nevertheless, the design of a real MCHP requires in any case the simultaneous optimization of the design of the AMR and magnet assembly.

In practice, this modularization strategy could be achieved by using three independent subsystems, each with its own magnet assembly, motor, and valve and fluid distribution/collection structure. The independent magnet assemblies could also share the same shaft in order to enable the use of a single motor to drive the whole system. If this is the case, the activation and deactivation of a module could be done using a clutch between the rotating part of each magnet assembly and the common shaft.

3.5. Seasonal COP

The SCOP was calculated based on the predefined operating points presented in Fig. 5 and considering the profile of the heating power demand shown in Fig. 3. The modularization strategy introduced in Section 3.4 was implemented in order to have an additional degree of freedom for the part-load capacity control of the MCHP. The SCOP depends on this modularization strategy (number of modules and number of AMRs per module) because for any given heating power demand value the operating point of the AMRs, and thus their COP, depends on the number of operating AMRs.

To explain the calculation procedure, let us consider the MCHP system consisting of 3 modules, one of 15 AMRs (module A), and two of 27 AMRs each (modules B and C). With these modules it is possible

Table 2
Some multi-bed MCHP systems developed in the last 15 years. The mass of the AMRs and the number of AMRs is presented.

Reference	N AMRs	AMR mass [g]	MCM	AMR Configuration	Magnet type
Huang et al. (2019)	7	169	Gd spheres	Flat disc	Rotating C-shape
Aprea et al. (2014)	8	150	Gd spheres	Flat disc	Rotating C-shape
Hai et al. (2024)	8	168	Gd particles	Cylinder	Rotating magnetic ring and iron core
Eriksen et al. (2015)	11	154	Gd and GdY	Cylinder	Rotating magnetic ring and iron core
Jacobs et al. (2013)	12	127	LaFeSiH particles	Unknown	Unknown
Dall'Olio et al. (2021)	13	262	LaFeMnSiH particles	Flat disc	Rotating magnet
Lozano et al. (2016)	16	106	Gd spheres	Cylinder	Magnetic rotor and iron stator
Engelbrecht et al. (2012)	24	117	Gd spheres	Rotating Cylinder	Concentric Halbach cylinders

to operate the MCHP with the following number of AMRs: 15, 27, 42, 54, or 69, corresponding to the operation of modules A, B (or C), A+B (or A+C), B+C, and A+B+C respectively. Then, for every heating power demand value, we first determine the minimum and maximum number of AMRs that must and could be in operation to supply the amount of heat under consideration. For example, a heating power demand of 550 W could be supplied using 15, 27, or 42 AMRs, in which cases every AMR would supply 36.7 W, 20.4 W, and 13.1 W respectively. The combination of modules corresponding to 54 AMRs cannot supply less than 629.9 W, so it cannot be considered for this heating power demand of 550 W. With these single-AMR heating capacities we obtain the cycle frequency, flow rate, and COP based on a piece-wise linear interpolation of the curves presented in Fig. 5. Using this approach for the present example, the COP values would be 4.5, 5.8, and 5.4 respectively. Therefore, for a heating power demand of 550 W, it is more efficient to operate with 27 AMRs since a higher COP is attainable. The same process is repeated for every heating power demand value in the range from 200 W to 3000 W using steps of 10 W, which gives a total of 281 values. These correspond to the heating power demand values obtained from the approach used to calculate the part-load heating power demand described in Section 3.1.

Fig. 6 shows the COP, AMR cycle frequency, and total volumetric flow rate obtained when following the calculation process described above for all considered heating power demand values. The total volumetric flow rate was calculated by multiplying the flow rate of a single AMR times the number of active AMRs times the blow fraction considered in this study, which is approximately equal to 28% (see Fig. 2). The discontinuities appreciable in Fig. 6 are due to the ON/OFF switching of AMR modules. It is relevant to mention that an automatic control of the MCHP will use flow rate as main control variable because it can be easily measured and because, as already mentioned, the capacity of an UFH system and a GSHEX can also be controlled by modulating the flow rate.

The SCOP is calculated as the weighted average of the COP values using the number of hours that every heating power demand value (or outdoor temperature) occurs as the weighting factor.

The distribution of COPs is shown in Fig. 7, and the calculated AMR SCOP is equal to 5.6 in this case. Fig. 8 shows the distribution of hours that the modules or combination of modules of AMRs would be in operation. It is clear that most of the time all modules operate, 3115 h, corresponding to heating power demand values above 1230 W. On the contrary, the MCHP operates with just 15 AMRs only 151 h, corresponding to heating power demand values below 400 W. A system SCOP can be estimated by considering representative efficiencies of motors and drive trains as proposed by Masche et al. (2023). If medium-efficiency equipment is taken into consideration, an overall equipment efficiency of 80% could be assumed (Masche et al., 2023), and the estimated system SCOP would be 4.5.

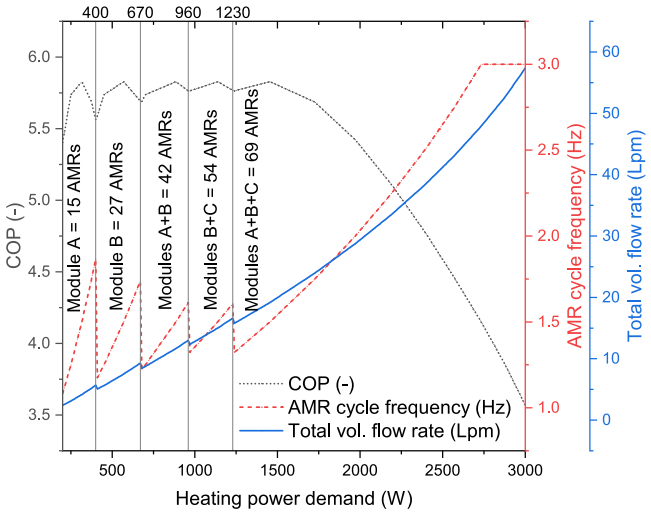

Fig. 6. COP, AMR cycle frequency and total volumetric flow rate as a function of total heating power demand for an MCHP with 3 modules, one module of 15 AMRs and two modules of 27 AMRs each.

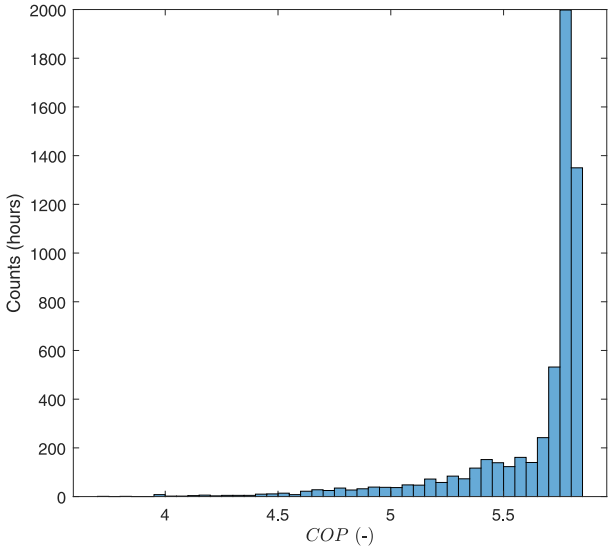

Fig. 7. Distribution of COPs for the heating season of the years 2009/2010 obtained when using modulation of flow rate and frequency as well as ON/OFF switching of modules of AMRs to control the capacity of the MCHP. The mean of this distribution is the seasonal COP, SCOP = 5.6.

3.6. Influence of number of modules and AMRs per module

Table 3 presents the SCOP obtained using several combinations of AMRs per module and number of modules. Here only odd numbers of AMRs per module are used, which limits the possible combinations. As can be seen in Table 3, the total number of AMRs was varied from 69 to 78. From this, it is possible to see a trend towards slightly higher SCOP values when larger numbers of AMRs are used. This comes from the fact that by using more AMRs the MCHP is a bit oversized, and thus in the high overall heating power demand range the AMRs do not have to operate near the point of maximum heating power, which coincides with the point of minimum COP. However, an increase of 13% of the

Table 3
SCOPs of different combinations of number of modules and AMRs per module.

Number of AMRs	Number of modules	AMRs per module	Operating AMRs by combination of modules	SCOP
70	2	[15, 55]	[15, 55, 70]	5.5
72	2	[17, 55]	[17, 55, 72]	5.6
69	3	[11, 29, 29]	[11, 29, 40, 58, 69]	5.6
69	3	[15, 27, 27]	[15, 27, 42, 54, 69]	5.6
71	3	[13, 29, 29]	[13, 29, 42, 58, 71]	5.7
70	4	[13, 19, 19, 19]	[13, 32, 38, 51, 57, 70]	5.6
72	4	[15, 19, 19, 19]	[15, 34, 38, 53, 57, 72]	5.7
75	5	[15, 15, 15, 15, 15]	[15, 30, 45, 60, 75]	5.7
77	7	[11, 11, 11, 11, 11, 11, 11]	[11, 22, 33, 44, 55, 66, 77]	5.7
78	6	[13, 13, 13, 13, 13, 13]	[13, 26, 39, 52, 65, 78]	5.7

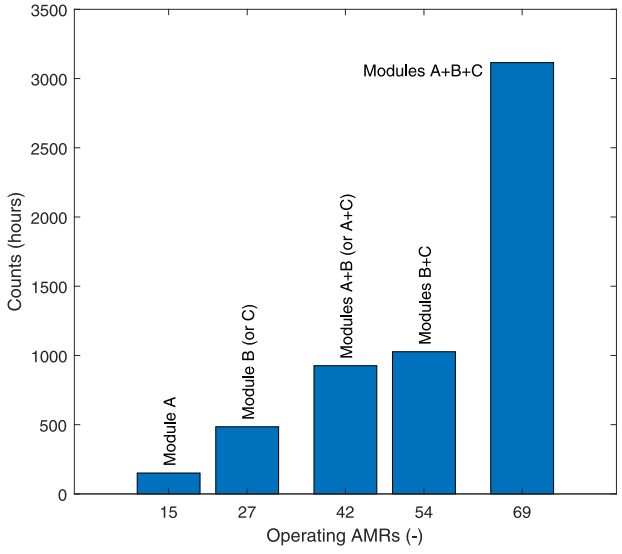

Fig. 8. Distribution of operating AMRs for the heating season of the years 2009/2010. The 5 possible combinations of the three selected modules (module A of 15 AMRs, module B and C of 27 AMRs) are shown in this figure.

number of AMRs only produces an increase of 3.6% of the SCOP. Thus, the enhancement is just marginal.

On the other hand, several numbers of modules were also tested for the same total number of AMRs. This allows to observe a trend towards higher SCOP values when more modules are used. For example, when using 70 AMRs divided in two modules, one of 15 and one of 55 AMRs, the SCOP is 5.5, but if the 70 AMRs are divided in 4 modules, one of 13 AMRs and three of 19 AMRs each, the SCOP is 5.6. This is due to the fact that in the low overall heating power demand range (below 1000 W) the heating power per AMR remains around the values for which the COP is maximum when the number of available AMRs increases progressively, e.g. from 13, to 32, to 38, and so on (see Table 3 row 6). On the contrary, when there is a large gap in the number of available AMRs, e.g. from 15 to 55, the heating power per AMR has to increase to the upper limit where the COP is lower.

From Table 3 it is also clear that the SCOP has a weak dependence on the number of modules and number of AMRs per module. This is related to the fact that the MCHP operates most of the time with all available AMRs as can be seen for example in Fig. 8. So, the modularization is mainly important for enabling the operation of the MCHP at low heating capacities. This suggests that the number of modules could be chosen following practical design reasons rather than performance reasons.

4. Conclusions

This article presents the calculation of the AMR SCOP of an MCHP for the built environment based on the MnFePSi material. A 12-layer AMR configuration with linear distribution of Curie temperatures and uniform length per layer was considered. A packed bed of spheres of 300 µm in diameter, 36% porosity, and overall dimensions $W \times H \times L = 45 \times 13 \times 60\,\mathrm{mm}^3$ was assumed. A maximum applied magnetic field strength of 1.4 T was considered as well as trapezoidal magnetic and fluid flow profiles. First, the performance of a single AMR was mapped using a 1D numerical model, i.e. the heating power and AMR COP was calculated for a fixed temperature span of 27 K and variable flow rate and AMR cycle frequency. Then, for every simulated flow rate value, the frequency that maximizes the COP and the corresponding heating power were found. In this way, it is possible to modulate the heating power of a single AMR from 11.66 W to 43.53 W following an optimum COP path by simultaneously changing the flow rate from $0.5\,\mathrm{L\,min^{-1}}$ to $3\,\mathrm{L\,min^{-1}}$ and the AMR cycle frequency from 1 Hz to 3 Hz. At least 69 AMRs are necessary to provide the design heating power demand of 3 kW considering the maximum heating power of a single AMR. Ambient temperature data of the Netherlands in the heating season of the years 2009/2010 were used to obtain a time dependent distribution of heating power demand values assuming a linear relationship between the heating power demand and outdoor temperature and a constant overall heat transfer coefficient and heat transfer area of the house, $UA = 100\,\mathrm{W\,K^{-1}}$. The pre-calculated optimum operating points were taken as a basis for the calculation of the SCOP. A modularization strategy was proposed to have an additional degree of freedom for controlling the capacity of the MCHP and enabling the reduction of the capacity of the MCHP to a minimum of 200 W. When considering the use of one module of 15 AMRs and two modules of 27 AMRs, the calculated AMR SCOP for the heating season of the years 2009/2010 is 5.6. If an efficiency of 80% is considered for motors and drive systems, an estimated system SCOP of 4.5 is obtained.

The main conclusions that can be drawn from this study are:

- The heating power capacity of a MCHP can be controlled efficiently by simultaneous modulation of the flow rate and AMR cycle frequency.
- Dividing a large MCHP system into modules is not only a wise solution from a practical perspective but also it is convenient to enable the reduction of the capacity of the heat pump to very small values. The overall heating power of the MCHP can be reduced efficiently to less than 10% of the design heating power by dividing the MCHP in modules, one of which should have a small number of AMRs to match the small heating power demand range.
- Flow rate is the preferred control variable in a MCHP system given that it is easy to measure for the implementation of a feedback control loop and given that the heating power of the MCHP and the UFH system and the heat transfer rate of the GSHEX can be modulated with this variable. AMR cycle frequency can be obtained from pre-calculated performance data so that the only control variable is the flow rate.
- Using an MCHP with a maximum heating power larger than the design heating power demand favours the SCOP given that the MCHP operates less hours at operating points where the COP is smaller.

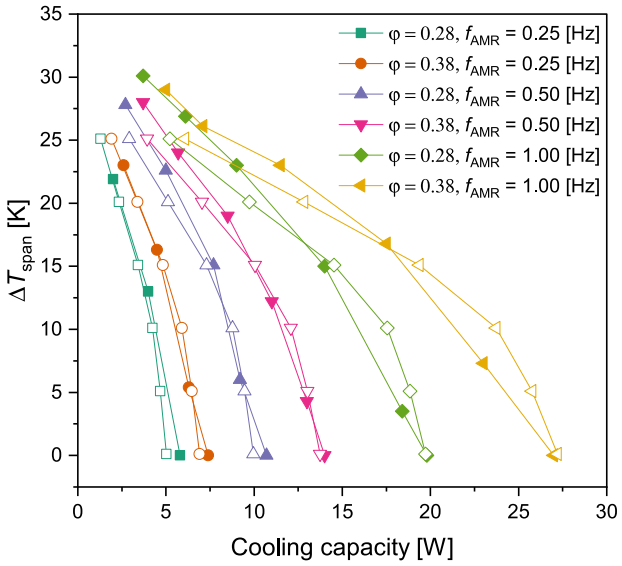

Fig. 9. Comparison of experimental and numerical results of simulations performed for the validation of the model. Performance data of a Gd-based, single-AMR device was used (Trevizoli et al., 2016b). Open symbols correspond to numerical results while solid symbols correspond to experimental data.

- The SCOP has a weak dependence on the number of modules and number of AMRs per module. This has to do with the fact that the MCHP operates with all available AMRs from medium to high heating power demand values, and most of the time in the heating season the heating power demand is in this range.

Furthermore, it is likely that by optimizing their design a fewer number of AMRs are needed to provide the same overall heating power demand. However, the modularization strategy should still be implemented in order to have greater flexibility in the control of the capacity of the MCHP to cover the full range of heating power demand values and to maximize the SCOP. Finally, a proper selection of pumps and motors as well as an efficient control of these devices is important to obtain a high system SCOP. Future work will include the validation of the performance predicted by the model using layered MnFePSi AMRs in the FAME cooler. Furthermore, the off-design performance of external heat exchangers should also be a matter of investigation. It is important to determine what is the most suitable design of an UFH system and a GSHEX for a proper operation in combination with a MCHP in a single hydraulic circuit given the wide range of flow rates at which the MCHP operates.

CRediT authorship contribution statement

Diego Pineda Quijano: Conceptualization, Formal analysis, Investigation, Methodology, Software, Writing – original draft. **Beatriz Fonseca Lima:** Investigation, Software. **Carlos Infante Ferreira:** Conceptualization, Formal analysis, Funding acquisition, Methodology, Supervision, Writing – review & editing. **Ekkes Brück:** Conceptualization, Formal analysis, Funding acquisition, Methodology, Project administration, Supervision, Writing – review & editing.

Declaration of competing interest

The authors declare that they have no known competing financial interests or personal relationships that could have appeared to influence the work reported in this paper.

Acknowledgements

This project is implemented with support from the MMIP 3&4 scheme of the Ministry of Economic Affairs & Climate Change and the Ministry of the Interior & Kingdom Relations of the Netherlands.

Appendix. Model validation

The model was validated using experimental data of a Gd-based, single-AMR device (Trevizoli et al., 2016b). A comparison between the experimental and numerical data is presented in Fig. 9.

References

Aprea, C., Greco, A., Maiorino, A., Mastrullo, R., Tura, A., 2014. Initial experimental results from a rotary permanent magnet magnetic refrigerator. Int. J. Refrig. 43, 111–122. http://dx.doi.org/10.1016/j.ijrefrig.2014.03.014.

Christiaanse, T.V., 2018. Characterization, Experimentation and Modeling of Mn-Fe-Si-P Magnetocaloric Materials (Ph.D. thesis). University of Victoria, Ph.D. thesis.

Christiaanse, T.V., 2019. An opensource active magnet regenerator model written in python. URL: https://github.com/TheoChristiaanse/AMRmodel.

Christiaanse, T.V., Trevizoli, P.V., Misra, S., Carroll, C., Van Asten, D., Zhang, L., Teyber, R., Govindappa, P., Niknia, I., Rowe, A., 2018. Experimental study of 2-layer regenerators using Mn-Fe-Si-P materials. J. Phys. D: Appl. Phys. 51 (10), http://dx.doi.org/10.1088/1361-6463/aaaba7.

Christiaanse, T.V., Trevizoli, P.V., Rowe, A., 2019. Modelling two layer Mn–Fe–Si–P materials in an active magnetic regenerator. Int. J. Refrig. 106, 225–235. http://dx.doi.org/10.1016/j.ijrefrig.2019.07.002.

Cozzi, L., Monschauer, Y., Wetzel, D., Bouckaert, S., 2022. The Future of Heat Pumps. Technical Report, International Energy Agency, Paris, URL: https://www.iea.org/energy-system/buildings/heat-pumps.

Dall'Olio, S., Masche, M., Liang, J., Insinga, A.R., Eriksen, D., Bjørk, R., Nielsen, K.K., Barcza, A., Vieyra, H.A., Beek, N.V., Bez, H.N., Engelbrecht, K., Bahl, C.R., 2021. Novel design of a high efficiency multi-bed active magnetic regenerator heat pump. Int. J. Refrig. 132, 243–254. http://dx.doi.org/10.1016/j.ijrefrig.2021.09.007.

Engelbrecht, K., Eriksen, D., Bahl, C.R., Bjørk, R., Geyti, J., Lozano, J.A., Nielsen, K.K., Saxild, F., Smith, A., Pryds, N., 2012. Experimental results for a novel rotary active magnetic regenerator. Int. J. Refrig. 35 (6), 1498–1505. http://dx.doi.org/10.1016/j.ijrefrig.2012.05.003.

Engelbrecht, K.L., Nellis, G.F., Klein, S.A., 2006. The effect of internal temperature gradients on regenerator matrix performance. J. Heat Transfer 128 (10), 1060–1069. http://dx.doi.org/10.1115/1.2345428.

Environmental Investigation Agency, 2015. EU F-Gas Regulation Handbook: Keeping Ahead of the Curve as Europe Phases Down HFCs. Technical Report, Environmental Investigation Agency, URL: https://eia-international.org/wp-content/uploads/EIA-F-Gas-Regulation-Handbook.pdf.

Ergun, S., 1952. Fluid flow through packed columns. Chem. Eng. Prog. 48 (2), 89–94.

Eriksen, D., Engelbrecht, K., Bahl, C.R., Bjørk, R., Nielsen, K.K., Insinga, A.R., Pryds, N., 2015. Design and experimental tests of a rotary active magnetic regenerator prototype. Int. J. Refrig. 58, 14–21. http://dx.doi.org/10.1016/j.ijrefrig.2015.05.004.

EU, 2023. Clean and efficient cooling - call for proposals. URL: https://eic.ec.europa.eu/eic-funding-opportunities/calls-proposals/clean-and-efficient-cooling_en.

European Committee for Standardization, 2022. Air conditioners, liquid chilling packages and heat pumps, with electrically driven compressors, for space heating and cooling, commercial and process cooling - testing and rating at part load conditions and calculation of seasonal performance (EN 14825:2).

Fortkamp, F.P., Eriksen, D., Engelbrecht, K., Bahl, C.R., Lozano, J.A., Barbosa, J.R., 2018. Experimental investigation of different fluid flow profiles in a rotary multi-bed active magnetic regenerator device. Int. J. Refrig. 91, 46–54. http://dx.doi.org/10.1016/j.ijrefrig.2018.04.019.

Goetzler, W., Zogg, R., Young, J., Johnson, C., 2014. Energy Savings Potential and RD&D Opportunities for Non-Vapor-Compression HVAC Technologies. Technical Report, U.S. Department of Energy, http://dx.doi.org/10.2172/1220817.

Hadley, G.R., 1986. Thermal conductivity of packed metal powders. Int. J. Heat Mass Transfer 29 (6), 909–920. http://dx.doi.org/10.1016/0017-9310(86)90186-9.

Hai, P., Shen, J., Li, Z., Li, K., Dai, W., 2024. Development and experimental analysis of a multi-bed active magnetic regenerator. Int. J. Refrig. 162, 169–178. http://dx.doi.org/10.1016/J.IJREFRIG.2024.03.015.

Huang, B., Lai, J.W., Zeng, D.C., Zheng, Z.G., Harrison, B., Oort, A., van Dijk, N.H., Brück, E., 2019. Development of an experimental rotary magnetic refrigerator prototype. Int. J. Refrig. 104, 42–50. http://dx.doi.org/10.1016/j.ijrefrig.2019.04.029.

Jacobs, S., Auringer, J., Boeder, A., Chell, J., Komorowski, L., Leonard, J., Russek, S., Zimm, C., 2013. The performance of a large-scale rotary magnetic refrigerator. Int. J. Refrig. 37, 84–91. http://dx.doi.org/10.1016/j.ijrefrig.2013.09.025.

Johra, H., Filonenko, K., Heiselberg, P., Veje, C., Dall'Olio, S., Engelbrecht, K., Bahl, C., 2019. Integration of a magnetocaloric heat pump in an energy flexible residential building. Renew. Energy 136, 115–126. http://dx.doi.org/10.1016/j.renene.2018.12.102.

Johra, H., Filonenko, K., Heiselberg, P., Veje, C., Lei, T., Dall'Olio, S., Engelbrecht, K., Bahl, C., 2018. Integration of a magnetocaloric heat pump in a low-energy residential building. Build. Simul. 11 (4), 753–763. http://dx.doi.org/10.1007/s12273-018-0428-x.

Kitanovski, A., Tušek, J., Tomc, U., Plaznik, U., Ožbolt, M., Poredoš, A., 2015. Magnetocaloric energy conversion - from theory to applications. p. 456. http://dx.doi.org/10.1007/978-3-319-08741-2.

KNMI, 2010. Hourly data of the weather in the Netherlands. URL: https://www.knmi.nl/nederland-nu/klimatologie/uurgegevens.

Koch, D.L., Brady, J.F., 1985. Dispersion in fixed beds. J. Fluid Mech. 154, 399–427. http://dx.doi.org/10.1017/S0022112085001598.

Lei, T., 2016. Modeling of Active Magnetic Regenerators and Experimental Investigation of Passive Regenerators with Oscillating Flow (Ph.D. thesis). Technical University of Denmark, p. 270, URL: https://orbit.dtu.dk/en/publications/modeling-of-active-magnetic-regenerators-and-experimental-investi.

Lei, T., Engelbrecht, K., Nielsen, K.K., Neves Bez, H., Bahl, C.R., 2016. Study of multi-layer active magnetic regenerators using magnetocaloric materials with first and second order phase transition. J. Phys. D: Appl. Phys. 49 (34), http://dx.doi.org/10.1088/0022-3727/49/34/345001.

Li, Z., Li, K., Guo, X., Gao, X., Dai, W., Gong, M., Shen, J., 2021. Influence of timing between magnetic field and fluid flow in a rotary magnetic refrigerator. Appl. Therm. Eng. 187, 116477. http://dx.doi.org/10.1016/j.applthermaleng.2020.116477.

Liang, J., Masche, M., Engelbrecht, K., Zhu, T., Bahl, C., 2022. The potential application of a magnetocaloric heat pump in ultra-low temperature district heating systems. In: ECOS 2022 - the 35th International Conference on Efficiency, Cost, Optimization, Simulation and Environmental Impact of Energy Systems. Copenhagen, pp. 1407–1418. http://dx.doi.org/10.11581/dtu.00000267.

Lionte, S., Risser, M., Muller, C., 2021. A 15 kW magnetocaloric proof-of-concept unit: Initial development and first experimental results. Int. J. Refrig. 122, 256–265. http://dx.doi.org/10.1016/J.IJREFRIG.2020.09.019.

Lozano, J.A., Capovilla, M.S., Trevizoli, P.V., Engelbrecht, K., Bahl, C.R., Barbosa, J.R., 2016. Development of a novel rotary magnetic refrigerator. Int. J. Refrig. 68, 187–197. http://dx.doi.org/10.1016/j.ijrefrig.2016.04.005.

Macias-Machin, A., Oufer, L., Wannenmacher, N., 1991. Heat transfer between an immersed wire and a liquid fluidized bed. Powder Technol. 66, 281–284. http://dx.doi.org/10.1016/0032-5910(91)80041-G.

Masche, M., Liang, J., Engelbrecht, K., Bahl, C., 2023. Efficient modulation of the magnetocaloric refrigerator capacity. Int. J. Refrig. 145, 59–67. http://dx.doi.org/10.1016/J.IJREFRIG.2022.10.005.

Nielsen, K.K., Tusek, J., Engelbrecht, K., Schopfer, S., Kitanovski, A., Bahl, C.R., Smith, A., Pryds, N., Poredos, A., 2011. Review on numerical modeling of active magnetic regenerators for room temperature applications. Int. J. Refrig. 34 (3), 603–616. http://dx.doi.org/10.1016/j.ijrefrig.2010.12.026.

Pineda Quijano, D., Infante Ferreira, C., Brück, E., 2023. Layering strategies for active magnetocaloric regenerators using MnFePSi for heat pump applications. Appl. Therm. Eng. 232, 120962. http://dx.doi.org/10.1016/J.APPLTHERMALENG.2023.120962.

Plaznik, U., Tušek, J., Kitanovski, A., Poredoš, A., 2013. Numerical and experimental analyses of different magnetic thermodynamic cycles with an active magnetic regenerator. Appl. Therm. Eng. 59 (1–2), 52–59. http://dx.doi.org/10.1016/j.applthermaleng.2013.05.019.

Qian, S., Yuan, L., Yu, J., 2019. An online optimum control method for magnetic cooling systems under variable load operation. Int. J. Refrig. 97, 97–107. http://dx.doi.org/10.1016/j.ijrefrig.2018.09.033.

Qian, S., Yuan, L., Yu, J., Yan, G., 2018. Variable load control strategy for room-temperature magnetocaloric cooling applications. Energy 153, 763–775. http://dx.doi.org/10.1016/j.energy.2018.04.104.

Romero Gómez, J., Ferreiro Garcia, R., De Miguel Catoira, A., Romero Gómez, M., 2013. Magnetocaloric effect: A review of the thermodynamic cycles in magnetic refrigeration. Renew. Sustain. Energy Rev. 17, 74–82. http://dx.doi.org/10.1016/j.rser.2012.09.027.

RVO, 2022. Voorbeeldwoningen 2022 Bestaande Bouw. Technical Report, Rijksdienst voor Ondernemend Nederland, URL: https://www.rvo.nl/sites/default/files/2023-01/brochure-voorbeeldwoningen-bestaande-bouw-2022.pdf.

Shirazi, A.S., Bernier, M., 2013. Thermal capacity effects in borehole ground heat exchangers. Energy Build. 67, 352–364. http://dx.doi.org/10.1016/j.enbuild.2013.08.023.

Smith, A., Bahl, C.R., Bjork, R., Engelbrecht, K., Nielsen, K.K., Pryds, N., 2012. Materials challenges for high performance magnetocaloric refrigeration devices. Adv. Energy Mater. 2 (11), 1288–1318. http://dx.doi.org/10.1002/aenm.201200167.

Trevizoli, P.V., Christiaanse, T.V., Govindappa, P., Niknia, I., Teyber, R., Barbosa, J.R., Rowe, A., 2016a. Magnetic heat pumps: An overview of design principles and challenges. Sci. Technol. Built Environ. 22 (5), 507–519. http://dx.doi.org/10.1080/23744731.2016.1171632.

Trevizoli, P.V., Nakashima, A.T., Peixer, G.F., Barbosa, J.R., 2016b. Performance evaluation of an active magnetic regenerator for cooling applications - part I: Experimental analysis and thermodynamic performance. Int. J. Refrig. 72, 192–205. http://dx.doi.org/10.1016/j.ijrefrig.2016.07.009.

Vieira, B.P., Bez, H.N., dos Santos, D., Lozano, J.A., Barbosa, J.R., 2023. Interrelationship between flow profiles and the magnetic waveform and their influence on the performance of first-order active magnetic regenerators. Appl. Therm. Eng. 219, 119581. http://dx.doi.org/10.1016/J.APPLTHERMALENG.2022.119581.

Wiesheu, M., Merkel, M., Sittig, T., Benke, D., Fries, M., Schöps, S., Weeger, O., Garcia, I.C., 2023. How to build the optimal magnet assembly for magnetocaloric cooling: Structural optimization with isogeometric analysis. Int. J. Refrig. 152, 62–73. http://dx.doi.org/10.1016/J.IJREFRIG.2023.04.014.